Characterization of the Sperm-Induced Calcium Wave in *Xenopus* Eggs Using Confocal Microscopy

Ray A. Fontanilla and Richard Nuccitelli
Section of Molecular and Cellular Biology, University of California, Davis, Davis, California 95616 USA

ABSTRACT We have used confocal microscopy to examine the $[Ca^{2+}]_i$ increase in the albino eggs of the frog *Xenopus laevis* after fertilization. Eggs were placed in agar wells with their animal poles downward so that fertilization occurred preferentially in the equatorial plane, and confocal microscopy was used to provide a two-dimensional optical section through the three-dimensional Ca^{2+} wave. These data indicate that the wave of increased $[Ca^{2+}]_i$ traverses the entire egg and converges uniformly on the antipode. We show that ratioing two different fluorescent dyes to correct for variations in cell thickness is not a reliable technique for this very thick cell due to differential absorption with depth. Indo-1-dextran proves to be a more reliable Ca^{2+} indicator in this respect. Indo-1-dextran measurements indicate that the resting $[Ca^{2+}]_i$ is not uniform throughout the egg but exhibits a 15% higher $[Ca^{2+}]_i$ in the cortex than deep in the cytoplasm. This difference is accentuated during wave propagation and is not dependent on extracellular Ca^{2+}. The average peak $[Ca^{2+}]_i$ in the center of the egg as the wave propagates through it is 0.7 μM, ~60% of the peak cortical $[Ca^{2+}]_i$. The wave velocity through the center of the egg (5.7 μm/s) is slower than that in the cortex (8.9 μm/s), and both velocities vary slightly during transit. The cortical wave speed is particularly high at the beginning (15.7 μm/s) and end (17.2 μm/s) of the wave. Eggs injected with 30–80 μM of 3 kD heparin to compete with inositol-1,4,5,-trisphosphate for binding to its receptor exhibited multiple localized spots of elevated $[Ca^{2+}]_i$, and many of these did not initiate a wave. For those that did lead to a wave, it was usually slow moving and exhibited a reduced (60% reduction) amplitude compared with controls.

INTRODUCTION

Xenopus laevis eggs, like those of all other species studied, display a transient increase in intracellular free calcium at fertilization (Whitaker and Steinhardt, 1982; Nuccitelli, 1991; Whitaker and Swann, 1993). This calcium increase begins at the site of sperm-egg fusion and travels across the egg until it reaches the point directly opposite the sperm entry site (antipode). The sperm-induced calcium wave has been previously described in the frog egg using calcium-selective microelectrodes (Busa and Nuccitelli, 1985) and fura-2 ratio imaging (Nuccitelli et al., 1993). The latter investigation, however, reported only the $[Ca^{2+}]_i$ within the outer layer of cytoplasm ~100 μM from the plasma membrane, as 80% of the fluorescence signal is emitted from that region and fluorescence from deeper cytoplasmic regions is greatly attenuated. Here we report the calcium release dynamics much deeper in the cytoplasm as the Ca^{2+} wave propagates along the equatorial plane of the 1.2-mm-diameter *Xenopus* egg using confocal microscopy.

MATERIALS AND METHODS

Obtaining gametes

Xenopus laevis eggs were obtained by gentle abdominal massage of females that had been induced to ovulate by the subcutaneous injection of 300–500 IU of human chorionic gonadotropin 8–10 h before the massage. Male frogs were anesthetized by surrounding them with ice and water for 50 min and then were decapitated and pithed. The testes were then removed and stored in OR2 (in mM: 82.5 NaCl, 2.5 KCl, 1.0 $CaCl_2$ 1.0 $MgCl_2$, 1.0 Na_2HPO_4, 5.0 Hepes, pH 7.8) at 4°C for up to 1 week.

Microinjection of eggs

Mature, jellied eggs were microinjected using an oil-filled line attached to a threaded syringe as previously described by Nuccitelli et al. (1993) with approximately 3 nl of 10 mM Ca-green-1-dextran (10,000 molecular weight) or some other dye in an intracellular injection buffer (in mM: 109 KCl, 5.0 HEPES, 5.0 $CaCl_2$, pH 7.3) to yield a final concentration of 60 μM inside the egg. Microinjection was conducted in a chlorobutanol solution (10% chlorobutanol) in calcium-free OR2 (in mM: 82.5 NaCl, 2.0 KCl, 5.0 HEPES, 20 $MgCl_2$, 0.1 EGTA, pH 7.4) to reduce the likelihood of activation of the eggs. Once injected, the eggs were held in the chlorobutanol solution for ~1 min and were then placed in F1 (in mM: 41.25 NaCl, 1.75 KCl, 0.5 $NaHPO_4$, 1.9 NaOH, 2.5 HEPES, 0.25 $CaCl_2$, 0.063 $MgCl_2$, pH 7.8) solution, and the injected dye was allowed to diffuse for 15–20 min. However, as indo-1-dextran requires the use of ultraviolet (UV) laser light, there are problems inherent in its use. UV light is absorbed by glass, so very thin coverslips and high NA objectives must be used. We found that the Zeiss 10× fluar objective with an NA of 0.5 was required to detect indo-1-dextran in *Xenopus* eggs. Dyes injected into eggs in this study included 5.6 nl of a solution of 7.5 mM calcium-green-1-dextran and 2.5 mM tetramethylrhodamine-dextran (10,000 molecular weight) to obtain a final concentration of ~60 μM and ~20 μM, respectively, within the egg for the purposes of ratio imaging. Some eggs were microinjected with 4.2 nl of 10 mM indo-1-dextran to a final concentration of ~90 μM.

Fluorescence imaging

The eggs were placed on a Zeiss LSM 410 inverted laser scan confocal microscope for all of the experiments described here. The Zeiss LSM 410 Invert was equipped with an argon/krypton excitation laser (Zeiss, 110 V,

Received for publication 18 March 1998 and in final form 17 June 1998.

Address reprint requests to Dr. Richard Nuccitelli, Molecular and Cellular Biology, University of California, Davis, One Shields Avenue, Davis, CA 95616-8535. Tel.: 530-752-3152; Fax: 530-752-7522; E-mail: rlnuccitelli@ucdavis.edu.

0006-3495/98/10/2079/09 $2.00

25 mW, 488/586 nm) and an UV laser (Coherent, 220 V, 351/364 nm). We used a 10× fluar lens (Zeiss, 0.5 NA) for all experiments. Filters for calcium-green-1-dextran were a 510-nm dichroic for excitation and a 515–555-nm BP for emission. Filters used for the double-dye staining with calcium-green-1-dextran and tetramethylrhodamine-dextran were a 488/568-nm dual dichroic for excitation, a 580-nm dichroic to split the fluorescence, a 515–555-nm BP for calcium-green-1-dextran emission, and a 590-nm long pass for tetramethylrhodamine-dextran emission. For the indo-1-dextran experiments we used a 345-nm dichroic for excitation, a 440-nm dichroic to split the fluorescence, and 460–510-nm BP and 395–435-nm BP for the dual emissions. A pinhole setting of 75 was used for all experiments. This gave an optical section thickness of 45 μm.

The indo-1-dextran fluorescence ratio image calibration curve was generated using a set of Ca^{2+} standards (Molecular Probes, Eugene, OR) placed in rectangular capillary tubes of 0.1-mm path length (Vitro Dynamics, Rockaway, NJ) with 90 μM indo-1-dextran. As the gain and black level varies for each experiment, assigning the calcium level to a given pixel intensity is problematic. However, we have extensive Ca^{2+} electrode measurements indicating that the average cortical $[Ca^{2+}]_i$ at the peak of the wave is 1.2 μM (Busa and Nuccitelli, 1985). Thus, we assigned this level to the peak cortical ratios and used the calibration curve to determine the lower values.

The albino egg was positioned in a petri dish chamber with a glass coverslip bottom coated with a 1-mm-thick layer of F1-agar. Hemispherical wells were made in the chamber using a warm glass rod with a spherical end that was the same size as a jellied egg. The jellied eggs were placed into the wells so that the best and most uniform signal was obtained. This was assumed to be with the animal hemisphere downward, facing the lens of the inverted microscope. This position should yield the least attenuation as the animal hemisphere has a lower concentration of yolk platelets than the vegetal hemisphere. Sperm was then added as a solution of 1/8 minced testis in 500 μl of F1 and images were recorded at 5-s intervals.

Wave analysis

Wave velocity measurements were made only on waves that both started and ended within the 40-μm-thick optical section at the equator of the egg. The Zeiss confocal LSM has the ability to determine signal intensity in a selected area called a region of interest (ROI). After determining the direction of wave propagation, we set up eight ROIs across the egg diameter or around the circumference.

The ROIs can be set to any size, but there is a trade-off between temporal resolution (small ROI) and signal noise due to fluctuation of individual pixel intensity. We found that a ROI of 16 × 16 (256) pixels provided the optimal signal-to-noise and temporal resolution for this velocity study.

A temporal scan of the ROIs produces a trace similar to that illustrated in Fig. 1. Each line represents the average pixel intensity in a ROI. As the wave front begins to pass through a ROI, the intensity increases. The signal continues to increase until the wave front completely passes through the ROI, at which point the signal levels out. To determine at what time the wave front passed through the ROI, we used the midpoint between the time the signal started to increase and the time the signal stopped increasing (representing the wave front "in" time and "out" time).

The wave propagation time between ROIs is calculated by subtracting the median time at which the pixel intensity increased in one ROI from the median time that it increased in the next ROI. The distance between ROIs is then divided by the corresponding interval time to give the interval velocity (μm/s). Total time and total distance were used to calculate the average velocity.

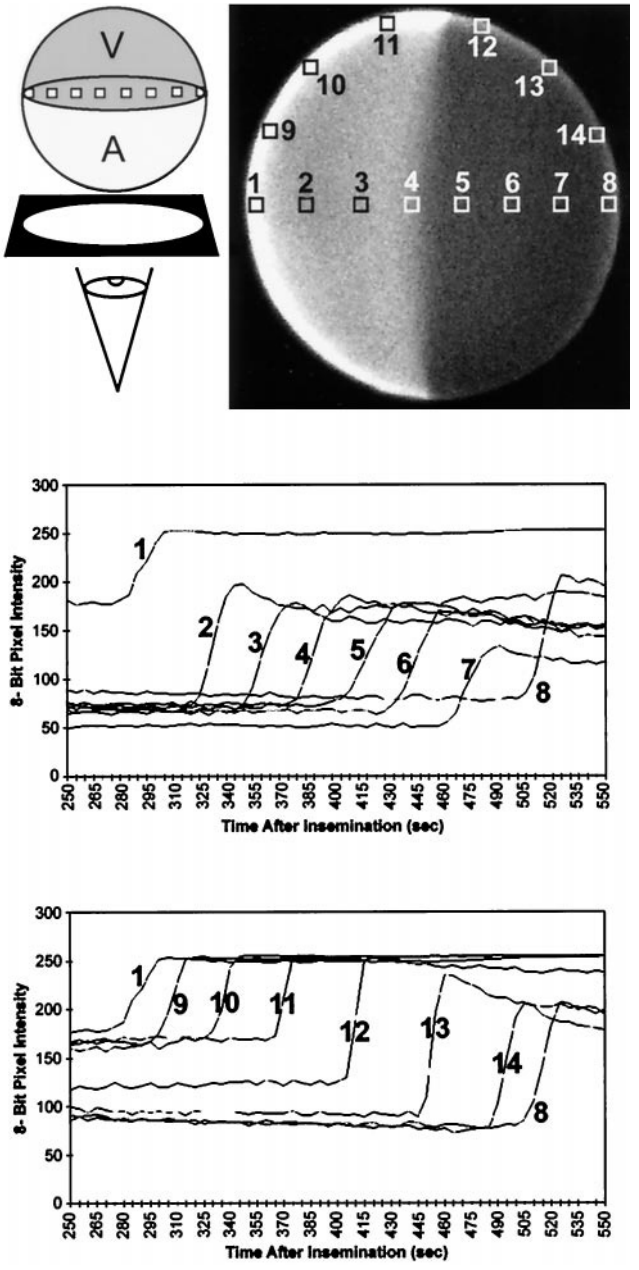

FIGURE 1 Velocity determination. (*A*) Egg orientation on the stage of the confocal microscope. We always placed the albino egg with its animal hemisphere downward, facing the lens. (*B*) A typical fluorescence image of the egg loaded with calcium-green-1-dextran with a calcium wave propagating through it. The numbered boxes indicate the typical placement of ROI boxes along the diameter of the egg. (*C*) Two typical ROI traces from the same egg after fertilization. Each numbered line corresponds to a numbered box in *B*. As the calcium wave passes through an ROI, the corresponding line trace increases, indicating an increase in calcium concentration.

RESULTS

The main goal of this study was to examine the fertilization-induced Ca^{2+} wave in the frog egg using confocal microscopy. We began with the fluorescent Ca^{2+} indicator, calcium green-1-dextran (Fig. 2). This gives a very bright signal and clearly indicated that the fertilization-induced Ca^{2+} wave propagates through the entire egg. This dye also does not interfere with normal development in any way. All embryos injected at the unfertilized egg stage with calcium-

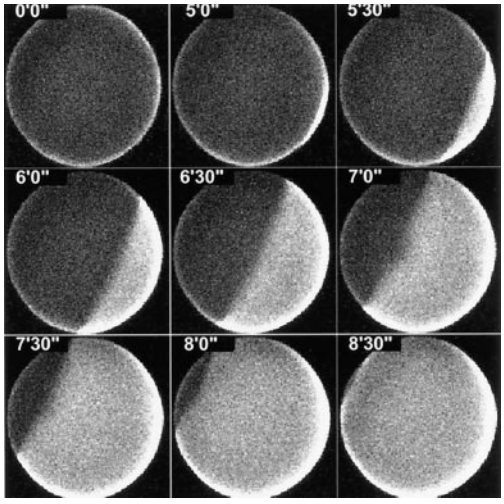

FIGURE 2 Calcium wave as observed using calcium-green-1-dextran. Dye was microinjected into a mature egg to a final concentration of ~60 μM within the egg. The image at time 0 shows the egg's resting level of calcium. Five minutes after sperm addition, the sperm-induced calcium wave began. Succeeding frames are at 30-s intervals. The average wave velocity is 5.6 μm/s in the center of the egg and 8.9 μm/s through the cortical region.

green-1-dextran developed to at least the blastula stage without much care, and several survived to the tadpole stage. Two of them are currently juveniles in our frog colony. It is quite evident that the fluorescence in the cortex appears brighter than that in the center region of the egg (Fig. 3). We will show below that this is largely due to an attenuation artifact because the path length of cytoplasm through which the fluorescence signal must pass is much shorter on the edge than it is in the center due to the spherical shape of the egg. Nearly all of the experiments described here involve the Ca^{2+} waves after normal fertilization. However, we also confirmed that ionophore (ionomycin)- and prick-activated waves propagate throughout the egg.

Double-dye ratio technique

We wanted to determine how much of the brightness difference between the egg center and the cortex was due to differential attenuation and how much was due to a real difference in $[Ca^{2+}]_i$. Our first approach was to use the double-dye ratio technique (Gillot and Whitaker, 1993). When calcium-green-dextran images were ratioed to the calcium-insensitive dye, tetramethylrhodamine-dextran (TMRD), we observed a much more uniform image throughout the egg. However, we discovered flaws in this technique that may apply only to very thick cells. Specifically, we found that the fluorescent signal from each dye is attenuated differently as it passes though the cytoplasm (Fig. 4). The fluorescent signal from TMRD is attenuated more with increasing cell thickness than that of calcium-green-1-dextran. That means that the ratio varies by ~25% as the depth of the optical section goes from the surface to 600 μm within the egg. This is probably due to a differential inner filter effect inherent in the two-dye approach. The two dyes are excited at 488 and 568 nm, respectively, and exhibit peak emissions at between 530 and 580 nm, respectively. Thus, it is quite possible that either the excitations or emissions of these two dyes are absorbed differently by cytoplasmic components as the light passes through the egg, which would generate a depth dependence in the ratio of signal intensities. Another possible complication is differential light scattering at the two wavelengths as well as

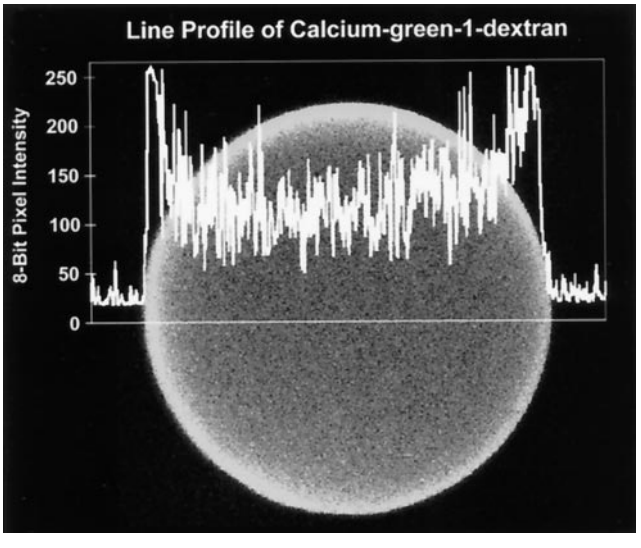

FIGURE 3 Plot of pixel intensity across an optical section taken through the middle of an unfertilized frog egg that had been microinjected with calcium-green-1-dextran. This histogram clearly displays a decreasing gradient of ~2.5-fold in apparent $[Ca^{2+}]_i$ between the edge and the center of the egg.

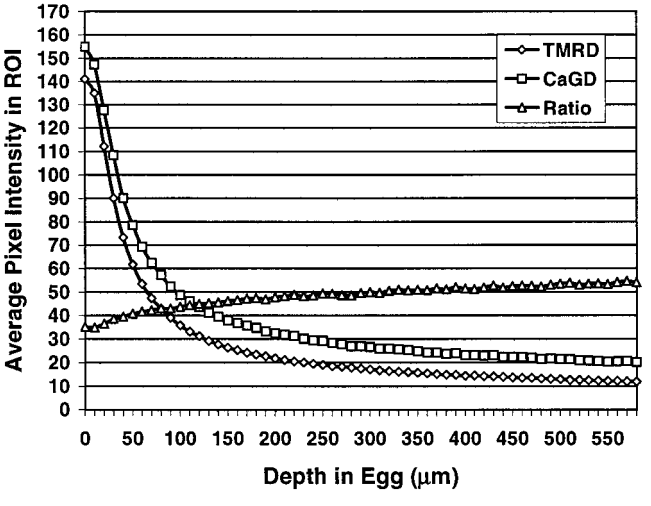

FIGURE 4 Average fluorescence intensity dependence on optical section depth in an albino *Xenopus laevis* egg. Tetramethylrhodamine-dextran fluorescence is absorbed more by the cytoplasm than that of calcium-green-1-dextran. The result is a variable ratio intensity with respect to the depth of the optical section.

differences in confocality at the two wavelengths arising from differences in the plane of focus if the microscope objective is not sufficiently corrected. Finally, we were concerned about the possible difference in distribution of the two dyes and the fact that TMRD blocked cleavage in *Xenopus* eggs. None of the 18 eggs injected with TMRD developed normally, whereas normal development was observed for all eggs injected with calcium-green-1-dextran alone. We noticed that even small amounts of TMRD caused the eggs to turn a pinkish color and cannot rule out the possibility that this disruption of development may have been due to an impurity in the TMRD we were using.

Using the ratioing dye indo-1-dextran

Because of these problems with the double-dye technique, we abandoned it in favor of using indo-1 dextran (10 kD). Indo-1 is excited at one wavelength in the UV, completely eliminating any worry of differential absorbance of the excitation, and emits fluorescence at two wavelengths, generating two images that can be ratioed (Figs. 5 and 6). When we studied the variation of these two signals with the depth of the optical section in the egg, we found a much less sensitive depth dependence than that observed using the double-dye technique (Fig. 7). The ratio varied by only 10% from 100 μm to 580 μm below the cell's surface. The rate of change of signal intensity with depth was greatest for all dyes used in the cortical region between 0 and 100 μm. The ratio also varied in this region, but for indo-1-dextran there was only a 4% variation compared with a 20% variation for the calcium green/TMRD pair. Therefore, we feel that the indo-1-dextran data are more reliable indicators of $[Ca^{2+}]_i$ than the two-dye technique. Two drawbacks to using indo-1-dextran are its requirements for UV excitation and an objective lens that will pass UV efficiently.

Interestingly, the ratio image from these eggs indicates that $[Ca^{2+}]_i$ levels in the unfertilized egg cortex still appear to be 15% higher than those in the regions deeper in the egg (Fig. 6; Table 1), and during the peak of the $[Ca^{2+}]_i$ wave the cortical levels are 70% higher (Fig. 8; Table 1). As these calcium values have been corrected for thickness by ratioing, it is likely that this difference is real and may reflect an asymmetry in the Ca^{2+} buffering system or endoplasmic reticulum Ca^{2+} stores, which have been found to be highly concentrated in the cortex (Charbonneau and Grey, 1984; Campanella et al., 1984).

Another possibility is that the $[Ca^{2+}]_i$ levels are higher in the cortex due to Ca^{2+} influx. To test this, we examined the intensity of the cortical $[Ca^{2+}]_i$ signal during the wave of increased free calcium before and after chelating the external Ca^{2+} by the addition of BAPTA to the medium outside the egg (Fig. 9). We could detect no significant difference in the cortical $[Ca^{2+}]_i$ levels before and after BAPTA addition and conclude that there is no detectable Ca^{2+} influx contributing to the apparently higher level of $[Ca^{2+}]_i$ in the cortex during wave propagation.

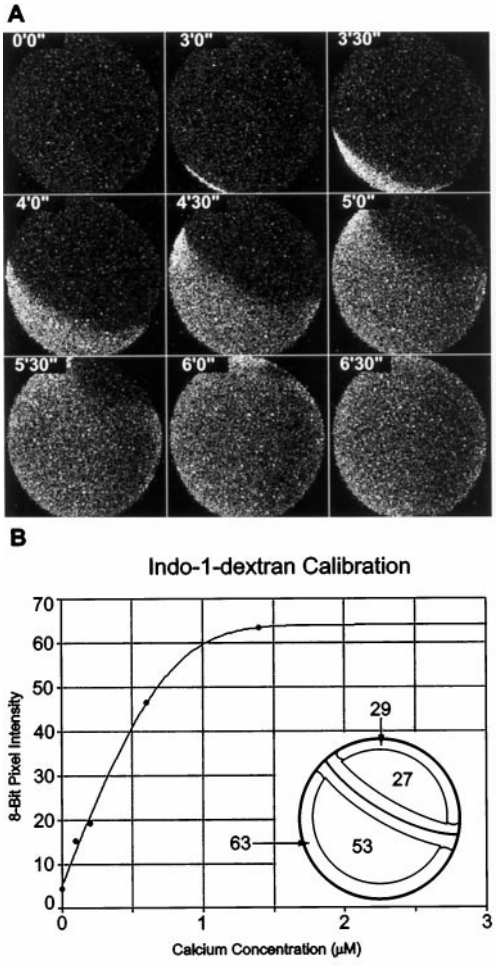

FIGURE 5 Calcium wave as detected using indo-1-dextran ratio imaging. (*A*) Top left frame shows the unfertilized egg's resting distribution of calcium. Directly to its right is the first sign of a sperm-induced calcium wave detected 3 min after sperm addition. Succeeding frames are at 30-s intervals after this frame. Images captured at 480- and 415-nm emission wavelengths were ratioed and confirm the hypothesis that much of the cortical brightness observed with calcium-green-1-dextran was due to less attenuation of the signal in the cortical region. (*B*) Indo-1-dextran fluorescence calibration curve using solutions of known calcium concentration. Numbers within the inset refer to the average pixel intensities observed within the regions diagrammed. We assigned the peak cortical $[Ca^{2+}]_i$ after fertilization a value of 1.2 μM based on Ca^{2+} microelectrode measurements and determined all other values from their relative pixel intensity on the calibration curve.

Properties Of the calcium wave

A careful examination of the Ca^{2+} wave pattern indicates that the wave travels more rapidly in the cortex than it does through the center of the egg (Fig. 10). The wave front through the center of the egg averages 5.7 μm/s, whereas the cortical wave front moves more rapidly at an average speed of 8.9 μm/s. Even more striking is the cortical wave velocity just after fertilization, which averages 15.7 μm/s, and that near the antipode, which averages 17.2 μm/s. This allows the wave front moving through the center of the egg to meet the cortical wave front just as they both reach the antipode.

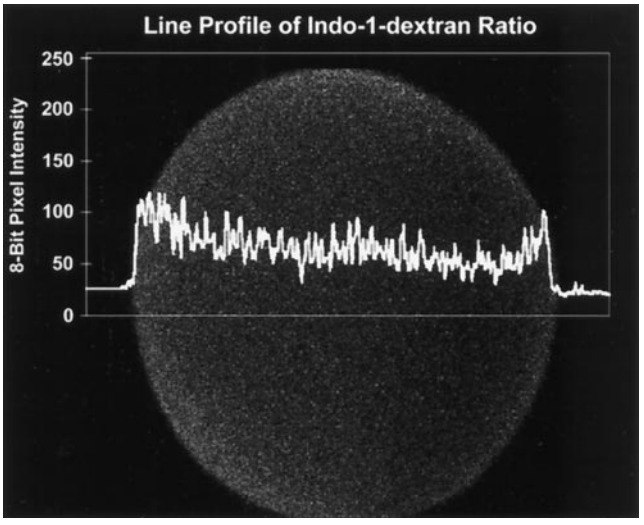

FIGURE 6 Plot of pixel intensity across an optical section taken through the middle of an unfertilized frog egg that had been microinjected with indo-1-dextran. The mean value of the intensity in the cortex is 15% higher than that in the center of the egg.

The wave amplitude is not uniform throughout the egg but appears to be higher in the egg cortex than at the center of the egg. The peak $[Ca^{2+}]_i$ in the egg center reaches only $\sim$0.7 μM, which is 60% of the peak cortical $[Ca^{2+}]_i$.

Heparin injection

In an effort to determine whether inositol-induced calcium release is involved in the mechanism of wave propagation, we injected eggs with 33–89 μM heparin (3 kD), which competes with inositol-1,4,5-trisphosphate ($Ins(1,4,5)P_3$) for binding to its receptor. Upon fertilization, these eggs displayed localized calcium increases in the cortical region ($n = 9$; Fig. 11). These hot spots lasted $\sim$5–6 min before recovering, and most did not propagate very far. Some of these eggs also displayed incomplete waves, in which the wave would start, propagate one-quarter to one-half through the egg, and then stop and fade away ($n = 5$; Fig. 11).

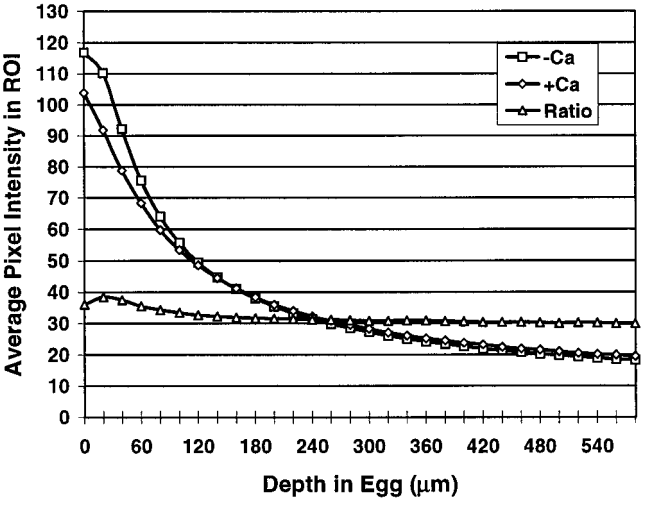

FIGURE 7 Average fluorescence intensity in a 16 $\times$ 16 pixel ROI at the two indo-1-dextran emission wavelengths with increasing depth of the optical section. Indo-1-dextran has significantly less differential attenuation than the double-dye technique. $\diamond$, intensity at the Ca^{2+}-sensitive wavelength; $\square$, intensity at the Ca^{2+}-insensitive wavelength. The result is a more accurate determination of the true calcium concentrations independent of cytoplasm path length. This result is representative of five different experiments.

TABLE 1 $[Ca^{2+}]_i$ in the cortex and central region of the frog egg

Position	Mean $[Ca^{2+}]_i \pm$ SD (μM)	
	Unfertilized egg	Peak of fertilization Ca^{2+} wave
Egg cortex	0.31 $\pm$ 0.03 ($n = 7$)	1.2
Central region	0.27 $\pm$ 0.03* ($n = 7$)	0.70 $\pm$ 0.03 ($n = 7$)

For each egg, the indo-1-dextran signal in the cortex during the peak of the Ca^{2+} wave was assigned the value of 1.2 μM, and the average peak $[Ca^{2+}]_i$ that was measured with a Ca^{2+}-selective electrode and the relative $[Ca^{2+}]_i$ values for the other regions were determined by scaling the calibration curve to this 1.2 μM value.
*Significantly different from the unfertilized egg value in the egg cortex according to the paired t-test ($p < 0.001$).

DISCUSSION

New findings

We present the first detailed study of confocal images of the sperm-induced calcium wave in the frog egg. These waves have been observed previously in a normal and a heparin-injected egg but were not described in detail (Galione et al., 1993; Whitaker, 1996). Our data indicate that this wave traverses the entire egg and converges uniformly on the antipode. We show that ratioing two different dyes to correct for variations in cell thickness is not a reliable technique for this very thick cell due to differential absorption of the excitation and emissions of the two dyes with depth. Indo-1-dextran proves to be a more reliable Ca^{2+} indicator in this respect. Indo-1 signals indicate that the resting $[Ca^{2+}]_i$ is not uniform throughout the egg but exhibits a slightly higher concentration (15%) in the cortex than deep in the cytoplasm. This difference increases to 70% during wave propagation and is not dependent on extracellular Ca^{2+}. The peak $[Ca^{2+}]_i$ in the center of the egg as the wave front passes through it is 0.7 μM compared with the 1.2 μM in the cortex. This is a very significant difference and might raise some doubt about the ability of Ca^{2+}-induced Ca^{2+} release (CICR) to contribute to the wave propagation through the center of the egg. However, previous work from our lab found that the center of the egg has the lowest threshold for CICR compared with both the animal and vegetal cortex (Nuccitelli et al., 1993). Eighty percent of *Xenopus laevis* eggs injected in their center with a Ca^{2+} buffer containing 0.8 μM free Ca^{2+} activated. Consequently, the endogenous levels of 0.7 μM are probably sufficient to trigger CICR and maintain wave propagation through that region.

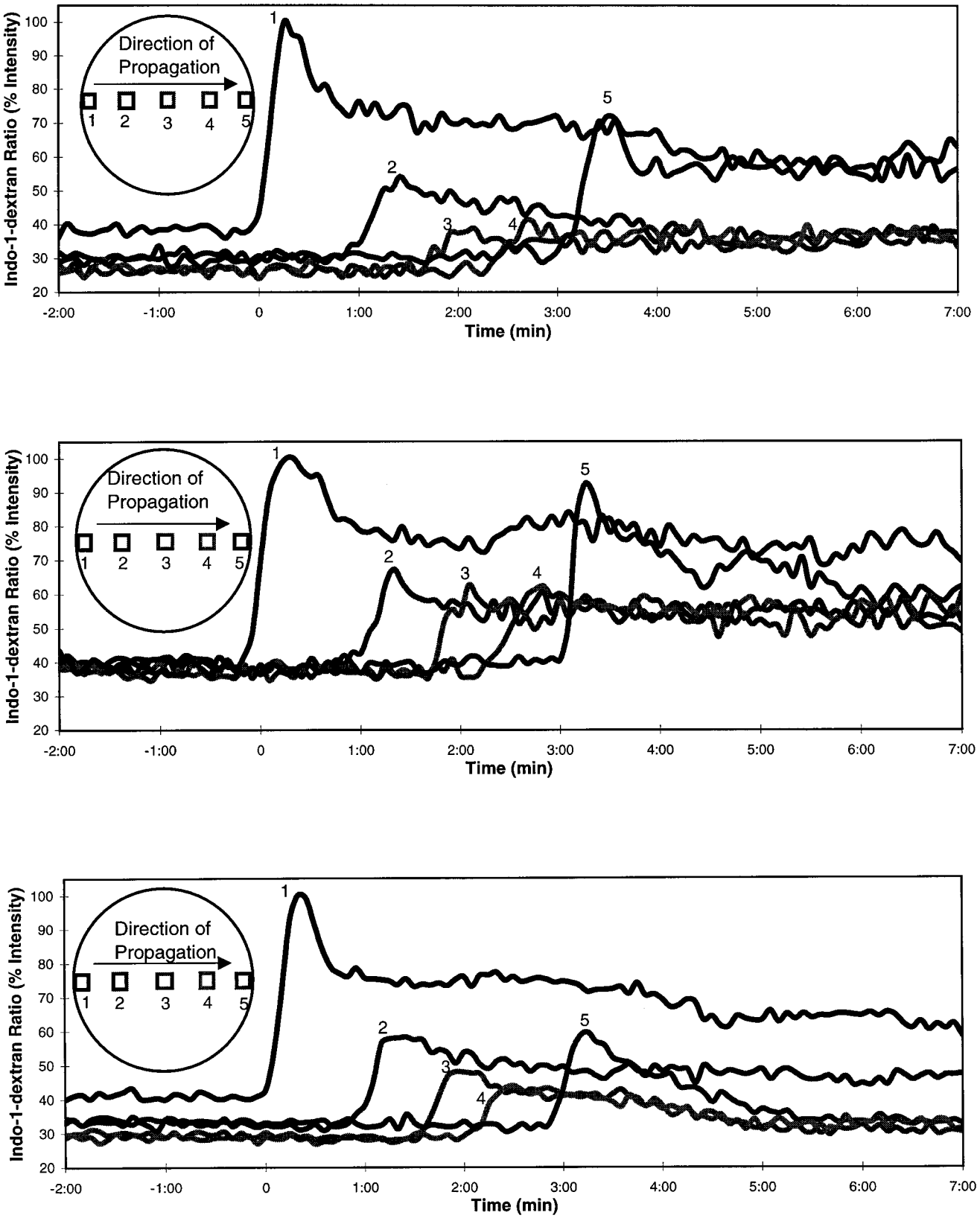

FIGURE 8 Time course of the $[Ca^{2+}]_i$ increase at different locations along the optical section through the center of an indo-1-dextran-injected egg. Analysis of the ratiometric images indicates that there is a significant difference in the level of calcium in the cortical region versus the center of the egg. Note that the ROI sizes in the inset are not to scale.

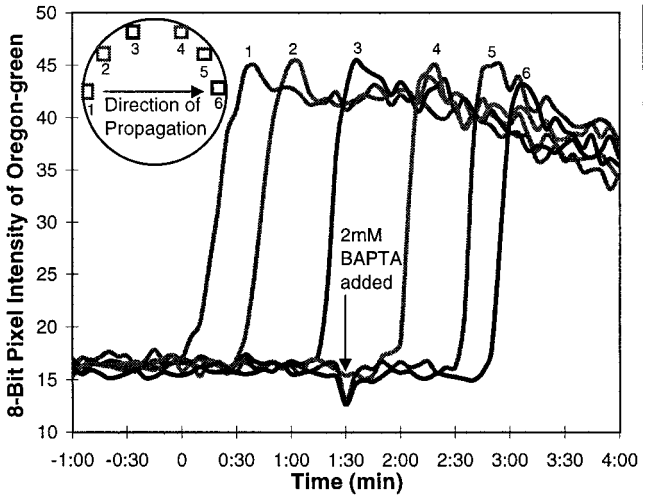

FIGURE 9 Chelation of external Ca^{2+} with BAPTA has no effect on cortical $[Ca^{2+}]_i$ increase. A mature albino egg was microinjected with Oregon-green dextran to a final concentration of 90 μM, and 100 μl of 30 mM BAPTA was added to 1.5 ml of F1 at the midpoint of the Ca^{2+} wave in the dejellied egg. There was no change in the $[Ca^{2+}]_i$ in the cortical region after extracellular Ca^{2+} was buffered to very low levels. Note that ROI sizes in inset diagram are approximate and not to scale. This result is representative of three different experiments.

The wave velocity through the center of the egg (5.7 μm/s) is slower than that in the cortex (8.9 μm/s), and both velocities vary slightly during transit. Eggs injected with 30–80 μM 3-kD heparin exhibited multiple hot spots or localized increases in $[Ca^{2+}]_i$, but most of these did not reach the level needed to trigger CICR. Those that did resulted in a slow-moving wave of reduced amplitude, suggesting that this wave of Ca^{2+} release is dependent in part on the occupation of the IP_3 receptor by Ins(1,4,5)P_3 rather than heparin.

These results indicate that the Ca^{2+} wave triggered by fertilization does indeed travel throughout the entire egg, rather than just along the surface. Interestingly, the wave always converges at the point opposite the sperm entry site (antipode). This is counterintuitive as the distance through the center of the egg is considerably shorter than the distance along the surface. This means that the cortical wave velocity is ~36% faster than that of the central wave spreading through the center of the egg. One would expect that uniform calcium release would generate a wave pattern similar to a ripple in a pond. Fig. 12 *A* assumes that a point source of Ca^{2+} at the sperm entry point diffuses outward with a regenerative CICR pattern rather than the pattern displayed by the activating egg illustrated in Fig. 12 *B*. This striking pattern is not intuitive and cannot be modeled by classical CICR (see accompanying paper, Wagner et al., 1998). As explained in that paper, this rapid initial speed is best modeled by a tangential gradient of Ins(1,4,5)P_3 production and a high concentration of cortical endoplasmic reticulum. We know that the latter is certainly the case

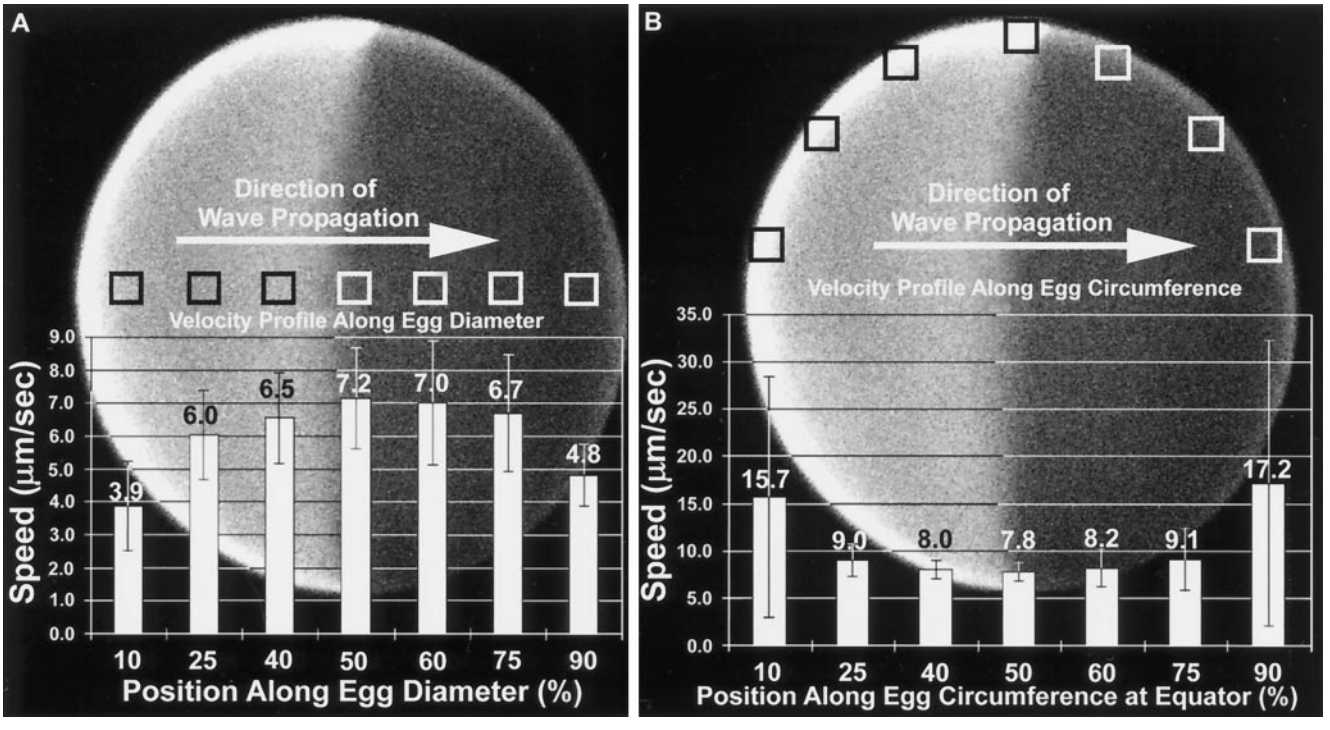

FIGURE 10 Average Ca^{2+} wave velocity profiles for ten albino *Xenopus* eggs. The *x* axis represents the relative position along the egg diameter (*A*) or circumference (*B*) at which the local wave velocity was determined. Values in the graph represent the local wave velocity as it crossed each square box indicated. Note that the wave velocity along the egg diameter appears to start out slowly, speeds up as it approaches the center, and then slows down again as it reaches the end. In contrast, the cortical wave exhibits a faster initial velocity, slows down as it approaches the center, and then speeds up again as it reaches the end.

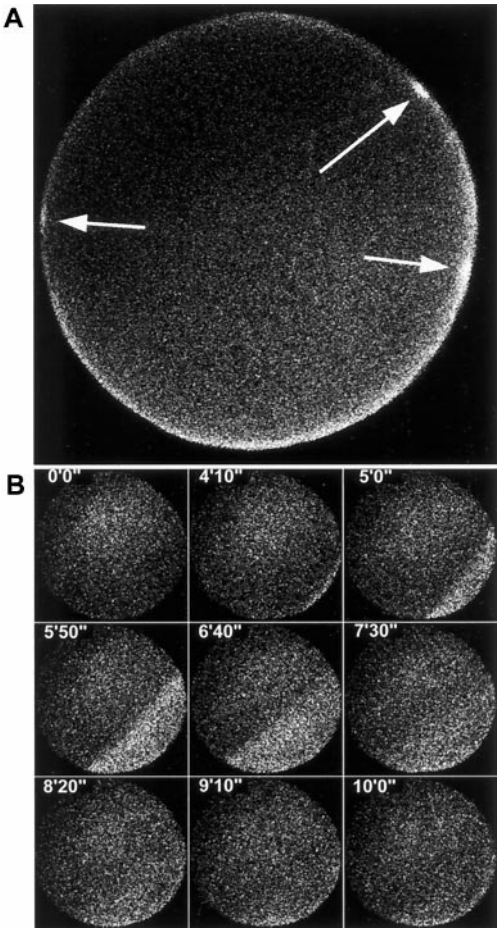

FIGURE 11 Effects of heparin on the sperm-induced calcium wave. Heparin is known to bind IP_3 receptors, thus disabling inositol-induced calcium release. (*A*) Typical multiple hot spot formation corresponding to multiple sperm fusion to the egg plasma membrane. Some eggs display many short-lived hot spots, whereas others display few long-lived hot spots. (*B*) Still other eggs display single or double slow-moving, incomplete waves. Also note that the intensity of fluorescence is often very light, indicating a very small calcium release.

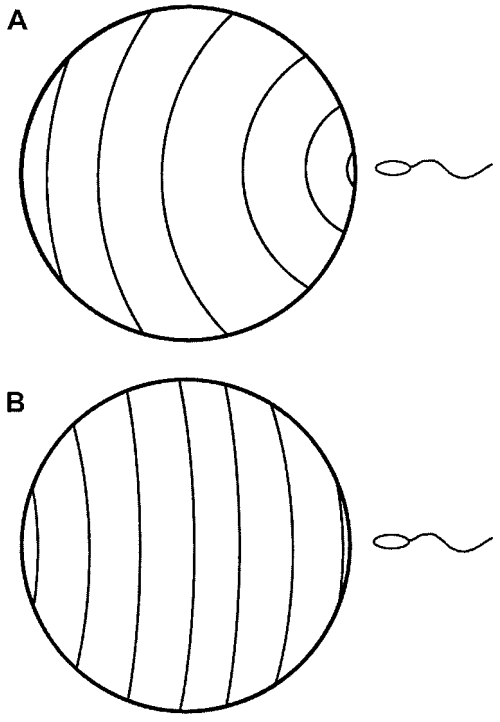

FIGURE 12 General wave dynamics. A wave begins at the position indicated by the sperm, which is presumably the sperm entry site. (*A*) Superimposition of calcium wave fronts expected as the wave travels across the egg assuming uniform calcium release. (*B*) The pattern of superimposed wave fronts actually observed.

because during maturation the density of the endoplasmic reticulum in the egg cortex increases dramatically (Campanella et al. 1984; Charbonneau and Grey, 1984). We suggest that the tangential Ins(1,4,5)P_3 gradient might be a result of the signal transduction cascade initiated by the sperm. The rapid speed of the cortical wave as it approaches the antipode can be explained by the geometry of the egg's plasma membrane in that region. Ca^{2+} accumulates at the boundary, increasing the Ca gradient as is evident in Figs. 2 *C* and 3 *C* in the accompanying paper (Wagner et al., 1998).

In an effort to determine the mechanism for the differences in wave velocities, we injected heparin to see what effects it would have on wave dynamics/velocity. Heparin is known to compete with IP_3 for binding to the IP_3 receptor, thus preventing inositol-induced calcium release. The cortical hot spots are probably sperm entry sites that caused localized calcium increases but did not increase the local $[Ca^{2+}]_i$ enough to induce activation and the blocks to polyspermy. This lack of a block to polyspermy allows multiple sperm entry sites, which are probably correlated with the multiple hot spots.

The fact that we can observe hot spots without accompanying Ca^{2+} waves suggests that there may be two separate Ca^{2+} release mechanisms involved here. We have recently observed that the sperm exhibits a surface protein in the metalloprotease, disintegrin, cysteine-rich (MDC) family and that cyclic peptides mimicking the disintegrin domain of this protein can trigger the Ca^{2+} wave upon local application to the egg (Shilling et al., 1997, 1998). This suggests that there may be a signal-transducing integrin in the egg's plasma membrane that is responsible for increasing the $[Ca^{2+}]_i$ locally and may contribute to the hot spot formation.

When waves are observed in the heparin-injected eggs, they have reduced amplitude and slower velocities than in control eggs. This suggests that Ins(1,4,5)P_3 levels can influence propagation velocity as well as the wave amplitude.

To summarize, we have described the propagation pattern of the Ca^{2+} wave in the frog egg that is initiated by fertilization. We find no dependence on extracellular Ca^{2+} and a strong dependence on inositol-induced calcium release. The initial cortical wave velocity is quite high and suggests that the sperm initiates Ins(1,4,5)P_3 production tangentially to cause the cortical Ca^{2+} release. The 70% higher $[Ca^{2+}]_i$ levels observed in the cortex during wave

propagation are consistent with the higher concentration of Ca^{2+} stores in that region and may contribute to the higher wave velocity observed there in comparison with deeper in the cytoplasm.

We thank Joel Keizer, John Wagner, Yue-Xian Li, and John Pearson for many stimulating discussions of this work and its interpretation.
This work was supported by National Institutes of Health Grant HD19966 to R. Nuccitelli and National Institutes of Health Grant RR10081 to Joel Keizer.

REFERENCES

Busa, W. B., and R. Nuccitelli. 1985. An elevated free cytosolic calcium wave follows fertilization in eggs of the frog *Xenopus laevis. J. Cell Biol.* 100:1325–1329.

Campanella, C., P. Andreucceti, C. Taddei, and R. Talevi. 1984. The modifications of cortical endoplasmic reticulum during in vitro maturation of *Xenopus laevis* oocytes and its involvement in cortical granule exocytosis. *J. Exp. Zool.* 229:283–293.

Charbonneau, M., and R. D. Grey. 1984. The onset of activation responsiveness during maturation coincides with the formation of the cortical endoplasmic reticulum in oocytes of *Xenopus laevis. Dev. Biol.* 102: 90–97.

Galione, A., A. McDougall, W. B. Busa, N. Willmott, I. Gillot, and M. Whitaker. 1993. Redundant mechanisms of calcium-induced calcium release underlying calcium waves during fertilization of sea urchin eggs. *Science*. 261:348–352.

Gillot, I., and M. Whitaker. 1993. Imaging calcium waves in eggs and embryos. *J. Exp. Biol.* 184:213–219.

Nuccitelli, R. 1991. How do sperm activate eggs? *Curr. Top. Dev. Biol.* 25:1–16.

Nuccitelli, R., D. L. Yim, and T. Smart. 1993. The sperm-induced Ca^{2+} wave following fertilization of the *Xenopus* egg requires the production of $Ins(1,4,5)P_3$. *Dev. Biol.* 158:200–212.

Shilling, F. M., J. Kratzschmar, H. Cai, G. Weskamp, U. Gayko, J. Leibow, D. G. Myles, R. Nuccitelli, and C. P. Blobel. 1997. Identification of metalloprotease/disintegrins in *Xenopus laevis* testis with a potential role in fertilization. *Dev. Biol.* 186:155–164.

Shilling, F. M., C. R. Magie, and R. Nuccitelli. 1998. Voltage-dependent activation of frog eggs by a sperm surface disintegrin peptide. *Dev. Biol.* In press.

Wagner, J., Y.-X. Li, J. Pearson, and J. Keizer. 1998. Simulation of the fertilization Ca^{2+} wave in *Xenopus eggs. Biophys. J.* 75:

Whitaker, M. 1996. Control of meiotic arrest. *Rev. Reprod.* 1:127–135.

Whitaker, M. J., and R. A. Steinhardt. 1982. Ionic regulation of egg activation. *Q. Rev. Biophys.* 15:593–666.

Whitaker, M., and K. Swann. 1993. Lighting the fuse at fertilization. *Development*. 117:1–12.